

Genetic algorithms predict formation of exotic ordered configurations for two-component dipolar monolayers†

Julia Fornleitner,^{*a} Federica Lo Verso,^{bc} Gerhard Kahl^a and Christos N. Likos^{bd}

Received 7th November 2007, Accepted 21st December 2007

First published as an Advance Article on the web 18th January 2008

DOI: 10.1039/b717205b

We employ genetic algorithms (GA), which allow for an unbiased search for the global minimum of energy landscapes, to identify the ordered equilibrium configurations formed by binary dipolar systems confined on a plane. A large variety of arrangements is identified, the complexity of which grows with increasing asymmetry between the two components and with growing concentration of the small particles. The effects of the density are briefly discussed and a comparison with results obtained *via* conventional lattice-sum minimization is presented. Our results can be confirmed by experiments involving Langmuir monolayers of polystyrene dipolar spheres or superparamagnetic colloids confined on the air–water interface and polarized by an external, perpendicular magnetic field.

Investigations of the structural and thermodynamic properties of colloids confined at fluid interfaces represent a very active topic of current research. Unlike particles in the bulk, the effective interactions between the colloidal particles at fluid interfaces are influenced not only by the properties of the particles and the solvent but, in addition, by the surface and line tensions of the interface.¹ Here we focus on the self-assembly scenarios of binary dipolar colloids, a system for which various experimental realizations exist, and whose interactions have been quantitatively established. Experimentally, studies of two-dimensional ordered arrangements of colloidal particles can be fairly easily realized by investigating polystyrene particles floating on an oil–water interface^{2,3} (system I). Their size, typically lying in the micrometre domain, allows a direct observation of the particles in light microscopes. Computer simulations for the binary case,⁴ mimicking the experimental setup sketched in Fig. 1(a), revealed a surprisingly rich spectrum of exotic ordered equilibrium structures. Another realization of such systems is offered by the setup of Maret and coworkers,^{5–9} employing superparamagnetic colloids suspended on a pendant water droplet, as sketched in Fig. 1(b) (system II). Here, a magnetic field **B** applied in the perpendicular direction polarizes the particles and induces a repulsive interaction

among them that scales with interparticle separation r as $\sim r^{-3}$, see ref. 9 and 10.

For system I, Sun and Stirner¹¹ have derived the following expressions for the pair potentials, $\Phi_{ij}(r)$, acting between the two species of particles:

$$\Phi_{ij}(r) = \begin{cases} \infty & r \leq (R_i + R_j) \\ \frac{P_i P_j}{16\pi\epsilon R_i R_j} \frac{1}{r} \ln \left[\frac{r^2 - (R_i - R_j)^2}{r^2 - (R_i + R_j)^2} \right] & r > (R_i + R_j) \end{cases} \quad (1)$$

$i, j = A, B.$

Here, R_i and P_i are the radius and the dipolar moment of species i and ϵ is the dielectric constant of water. In what follows, we assume that $P_i = \alpha R_i^3$, with some proportionality constant¹² α . Introducing $z \equiv R_B/R_A < 1$ and $x \equiv r/d_A$ ($d_A = 2R_A$), and factoring out a prefactor common to all three interactions $\Phi_{ij}(r)$, we arrive at the following expressions for the dimensionless interaction potentials $\Psi_{ij}(x)$:

$$\Psi_{AA}(x) = \frac{1}{x} \ln \left[\frac{x^2}{x^2 - 1} \right] \quad \text{for } x \geq 1; \quad (2)$$

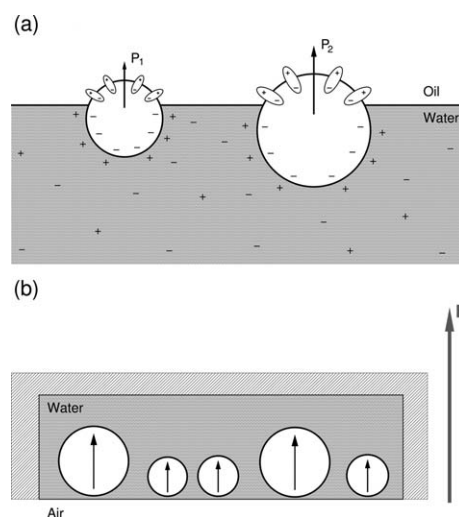


Fig. 1 (a) Schematic representation of system I (inspired by ref. 4): two particles of different size floating at an oil–water interface. The dipole moments P_1 and P_2 are given by the vector sum of the dipole moments on the particle–oil interface, since the dipole interaction is screened in the aqueous phase. (b) Schematic representation of system II: superparamagnetic colloidal particles trapped on the water–air interface in a pendant water droplet. The external magnetic field **B** is used to tune the interactions between the spheres.

^aCenter for Computational Materials Science and Institut für Theoretische Physik, Technische Universität Wien, Wiedner Hauptstraße 8–10, A-1040 Vienna, Austria

^bInstitut für Theoretische Physik II: Weiche Materie, Heinrich-Heine-Universität Düsseldorf, Universitätsstraße 1, D-40225 Düsseldorf, Germany

^cChimie Analytique et Biophysico-chimie de l'Environnement (CABE), Université de Genève - Sciences II, 30, Quai Ernest-Ansermet, CH-1211 Genève 4, Switzerland

^dThe Erwin Schrödinger International Institute for Mathematical Physics (ESI), Boltzmannstraße 9, A-1090 Vienna, Austria

† The HTML version of this article has been enhanced with colour images.

$$\Psi_{BB}(x) = \frac{z^3}{x} \ln \left[\frac{x^2}{x^2 - z^2} \right] \quad \text{for } x \geq z; \quad (3)$$

$$\Psi_{AB}(x) = \frac{z^{3/2}}{x} \ln \left[\frac{4x^2 - (1-z)^2}{4x^2 - (1+z)^2} \right] \quad \text{for } x \geq (1+z)/2. \quad (4)$$

The functions $\Psi_{ij}(x)$ are displayed in Fig. 2(a) for two different values of z . Expanding the logarithms for $x \gg 1$ yields the approximate expressions $\Psi_{ij}(x) \cong (z_{ij})^{5/2}/x^3$, where $z_{ij} = 1$ or z if $i, j = A$ or B . Fig. 2(b) shows the asymptotic, power-law form of the interactions. In two dimensions, where the exponent of the power-law exceeds the dimension of space, the subtle issues of the shape-dependence of the thermodynamics, which arise for *three-dimensional* dipoles,¹³ are absent.

For system II, on the other hand, where the superparamagnetic colloids have a susceptibility ratio $m < 1$, the dimensionless interaction potentials read^{9,10,14} as $\psi_{ij}(x) = m_{ij}m/x^3$, where $m_{ij} = 1$ or m if $i, j = A$ or B . If the overall density of system I is sufficiently low, so that the asymptotic forms of $\Psi_{ij}(x)$ above hold, systems I and II become equivalent, with the correspondence $z^{5/2} \leftrightarrow m$. The ground states of system II have been recently analyzed with conventional

methods in the work of Assoud *et al.*¹⁴ for $0.08 \leq m \leq 1$, being inspired by the phase diagram of a two dimensional, binary hard-sphere mixture.¹⁵ Here, we concentrate on system I in the domain $0.1 \leq z \leq 0.5$, corresponding to much stronger asymmetries (*i.e.*, $3 \times 10^{-3} < m < 0.18$) but still having sufficient overlap in the parameter range with that of ref. 14 to allow for quantitative comparisons. Finally, the system is characterized by the number-density η or its dimensionless counterpart, ηd_A^2 .

It is well-known that binary mixtures tend to show a broad spectrum of rather complex alloy phases, most of them being extremely hard to guess. With the ambition to cover as large a variety of structures as possible and in an effort to cope with this problem in an efficient way, we employed genetic algorithms¹⁶ (GAs) instead of following the conventional approach to the problem of finding minimum energy configurations (MECs), which relies on preselected sets of candidate structures. GAs were invented in the 1970s by Holland to solve high dimensional and complex problems in engineering science.¹⁷ They are optimization techniques, modeled after the natural process of evolution, and mimic certain biological mechanisms, such as mating and mutation, to find the optimal solution to a proposed problem. Due to its special design, a GA is able to take the whole search space into account at once and at the same time to concentrate its computing efforts on promising regions. It is this *global scope* that makes GAs an efficient and widespread tool in fields like economics and engineering. In the realm of structure optimization, a typical problem in atomic condensed matter physics, they have found applications in determining optimal atomic clusters,^{18,19} and, very recently, in optimizing extended spatial structures.²⁰⁻²² In soft matter, applications of GAs to predict equilibrium crystal structures for one-component systems has already delivered remarkable results, both in two²³ and three dimensions,²⁴⁻²⁶ but binary systems have not been looked upon with GAs so far.

Based on the approaches presented in ref. 27, we designed a method to determine ordered MECs for binary monolayers. In our method, lattice parameters are freely optimized with respect to the free energy, which, at $T = 0$, reduces to the lattice sum U of the ordered structure. The efficiency of the GA allows us to perform our search for equilibrium structures among all possible lattices, without posing any bias on the algorithm whatsoever. The only limiting factor constraining our search is the maximum of particles per cell that the algorithm can handle in a reasonable time. The risk of overlooking relevant structures at any point in the process is thus minimized.

In general, we have to deal with non-Bravais lattices, with $s (> 1)$ particles per unit cell. We parametrized these lattices with n_A particles in the unit cell belonging to species A and the remaining $n_B = s - n_A$ particles to the other species, B, coding the position vectors of all particles in a binary fashion. We obtained results for particle size ratios in the range of $z = 0.1$ to $z = 0.5$, including the value of $z = 0.3296$ that corresponds to the particle size ratio used in previous Monte Carlo (MC) simulations.⁴ The concentration of small particles, $C = n_B/s$, was systematically varied for every size ratio. Most of the calculations were performed with a maximum of eight particles per unit cell, so C lay in the range $1/8 \leq C \leq 7/8$. Additional calculations were performed for $C = 7/9$, as exotic phases were to be expected for this particular ratio.¹⁵

Before presenting the results obtained by the GA, let us discuss some generic expected features of the MECs, arising from the functional form of the potential. In sufficiently dilute one-component

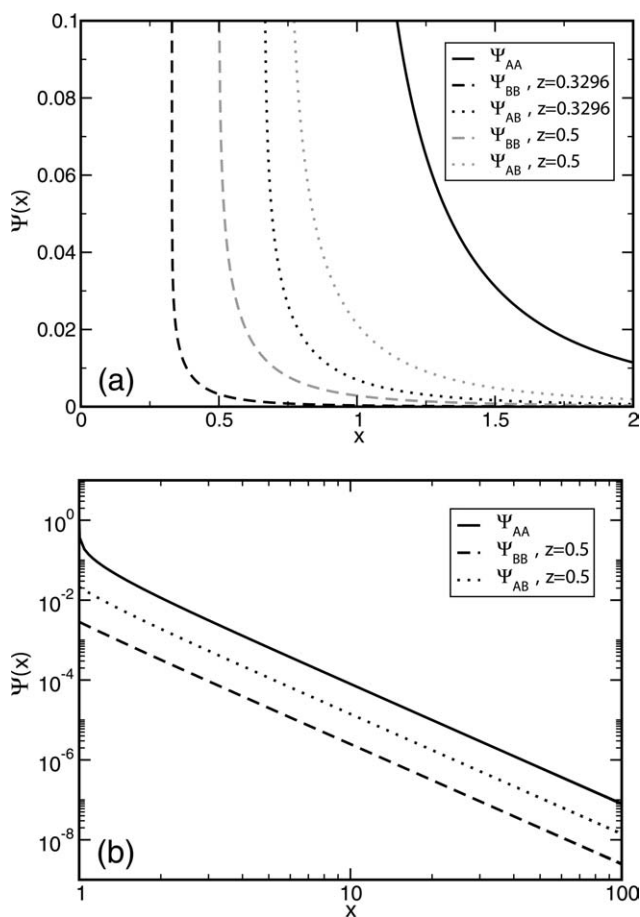


Fig. 2 (a) The interaction potentials of eqn (1) for $z = 0.3296$ (full lines) and $z = 0.5$ (broken lines). (b) Double logarithmic plots of $\Psi_{ij}(x)$ for $z = 0.5$, demonstrating their $\sim x^{-3}$ power-law dependence for large x -values.

systems, a hexagonal lattice is formed since $\Psi_{ij}(r) \sim r^{-3}$ at long distances. This “default structure” is also found in two limiting cases of the binary mixture: first, for $z \rightarrow 0$, when the smaller B-particles are of vanishing size compared to the larger A-particles, and second for $z \rightarrow 1$, when the two species become indistinguishable. In the first case we expect the large particles to form hexagonal lattices, more or less unperturbed by the presence of the small ones. If z is small, the B-particles can form independent patterns in the interstitial regions of the hexagonal lattice formed by the A-particles without paying a high

penalty in energy. Thus, distinct groups of small particles should be observed with their size fulfilling the stoichiometric requirements. In the opposite case, as the similarity in size increases, the B-particles require more space. Now the concentration and the dependence of the interspecies interactions on the distance are the key quantities that determine the ordered equilibrium structure.

In Fig. 3 and 4 we present the ordered equilibrium configurations found with our GA-method for increasing concentration of small particles C at an overall particle density of $\eta d_A^2 = 0.6$. To facilitate

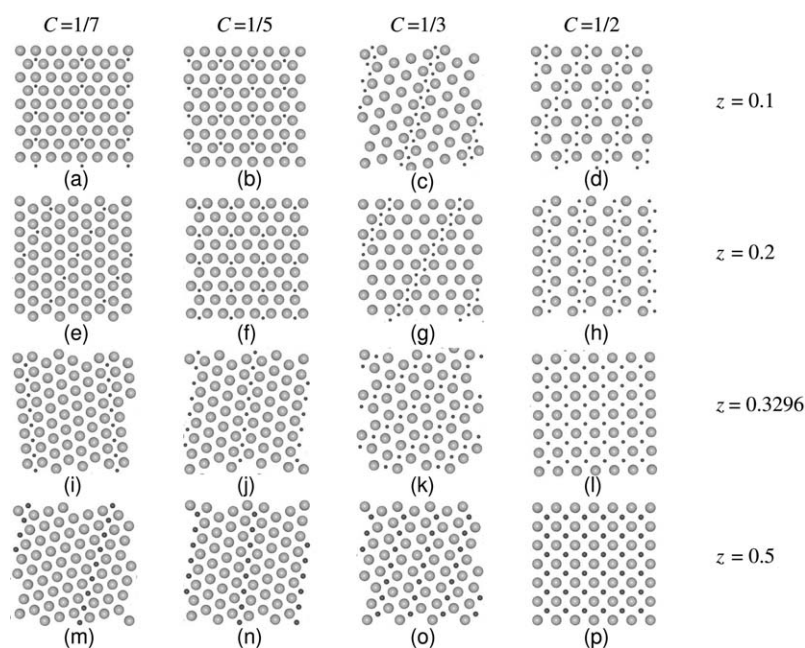


Fig. 3 Minimum energy configurations for $C \leq 1/2$, i.e. $n_B \leq n_A$ for $\eta d_A^2 = 0.6$. Particle diameters are not drawn to scale.

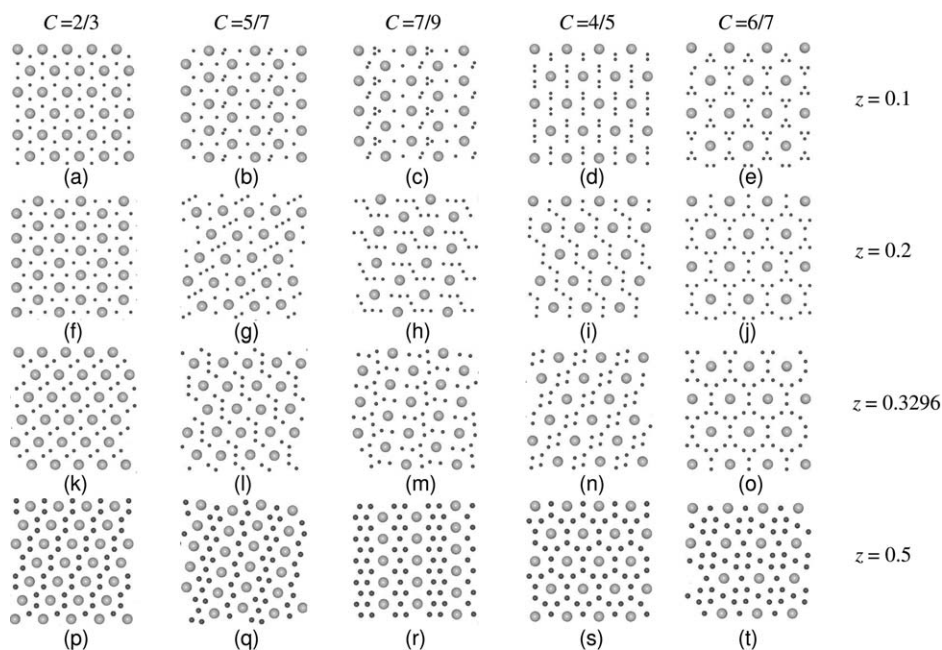


Fig. 4 Minimum energy configurations for $C > 1/2$, i.e. $n_B > n_A$ for $\eta d_A^2 = 0.6$. Particle diameters are not drawn to scale.

discussion we divide our results into two blocks: structures with $n_B \leq n_A$ (Fig. 3) and structures $n_B > n_A$ (Fig. 4). We begin with the case $n_B \leq n_A$. For sufficiently large values of z , *i.e.*, $z = 0.3296$ and $z = 0.5$, the small particles are able to perturb the (ideal) hexagonal structure formed by the large particles in their immediate surrounding, even though they represent the minority component. In regions where there are no small particles in the immediate neighborhood, the hexagonal structure of the large particles prevails, whereas the small particles are found in the center of squares formed by the large particles [see Fig. 3(i), (j), (m) and (n)]. On the other hand, if z is below a certain threshold, *i.e.*, $z = 0.1$ and $z = 0.2$, the influence of the small particles is not sufficient to cause a substantial modification of the hexagonal pattern of the large particles. Instead, since the small particles experience mutually a very weak repulsion, they tend to stay close together in this z -regime, arranging in lanes which meander through the hexagonal lattice formed by the large particles, see Fig. 3(c), (d), (g) and (h). For very small concentrations, *i.e.*, $C = 1/7$ and $C = 1/5$ [*cf.* Fig. 3(a), (b), (e) and (f)], the ‘lanes’ of the small particles are interrupted by intervening big ones due to the simple fact that not sufficiently many B-particles are available in the system. It might be possible that also in these cases pure B-particle lanes will form but this would require a much larger unit cell, which was not included in our study.

When the small particles become the majority component, the found structures become much more complex, as can be seen from Fig. 4. As expected, B-particles are observed to arrange in distinct groups for many parameter settings. We find small particles forming dimers, [Fig. 4(b), (c) and (d)], elongated- [Fig. 4(g)] and triangular-trimers [Fig. 4(c) and (e)], as well as chain-like pentamers [Fig. 4(l)] and heptamers [Fig. 4(h)]. In contrast, the A-particles form rather simple lattices which accommodate in their interstitial regions these sometimes rather complex groups of B-particles. For $C = 2/3$, dimers of small particles, observed for moderate values of z [Fig. 4(k)] are a precursor of lane formation [Fig. 4(p)]. For small values of z , the large particles form a hexagonal pattern and the small particles are distributed in the interstitials. At $z = 0.3296$ the hexagonal structure of the large particles is distorted and the small particles are grouped in dimers. If the particle size ratio is further increased, the dimers of small particles change their orientation and lane formation sets in which now strongly distorts the underlying lattice of A-particles. The scenario repeats itself for $C = 5/7$, [vertically from Fig. 4(b) to Fig. 4(q)] but here the stoichiometry, which does not accommodate a single B-particle in the interstitials of A, forces a much richer structure: for $z = 0.1$, Fig. 4(b), the B-particles form an ordered array of monomers and dimers, which transforms into an array of monomers and linear trimers for $z = 0.2$, Fig. 4(g). For $z = 0.3296$, the aggregates of B-particles become monodisperse, zig-zag-like pentamers, Fig. 4(l); and, finally, for $z = 0.5$, formation of two interchanging kinds of B-lanes, thick and thin, takes place, Fig. 4(q).

Evidently, the higher the value of C , the more surprises the system has to offer. Let us discuss the sequences for $C = 7/9$, $C = 4/5$, and $C = 6/7$ in more detail. For $C = 7/9$ and for small z -values, the interstitials of the A-lattice are occupied by *three different kinds* of B-aggregates: monomers, dimers and triangular trimers, Fig. 4(c). For $z = 0.2$, B-particles arrange in zigzag-shaped heptamers which distort the hexagonal pattern of the large particles, Fig. 4(h). However, in contrast to the smaller C -values a further increase of z does not directly lead to lane formation but rather a new, exotic structure intervenes for $z = 0.3296$, Fig. 4(m). Here, two neighboring

heptamers merge, forming thereby a sequence of alternately oriented cup-like structures, each of them hosting an A-particle. If z is increased further, thick and thin lanes are again formed, Fig. 4(r). In the second sequence, $C = 4/5$, the B-dimers [Fig. 4(d)], observed for $z = 0.1$, transform into zig-zag lanes [Fig. 4(i)], pearl-necklace-lanes [Fig. 4(n)] and finally into rings, each of them surrounding one A-particle, [Fig. 4(s)], as z grows. Finally, for the sequence $C = 6/7$, a ring-like structure is formed for $z = 0.1$ to $z = 0.3296$, Fig. 4(e), (j) and (o), where every large particle is surrounded by six triangular trimers of small particles, forming a structure resembling a Kagome lattice [Fig. 4(e)]. The B-interparticle distance *within* the trimers increases with z . Finally, for $z = 0.5$ lane formation sets in once more [Fig. 4(t)], but now the lanes formed by the small particles are interconnected, due to the high concentration of B-particles.

The structures found by the GA for $z = 0.5$ correspond to $m = 0.177$ in the terminology of Assoud *et al.*¹⁴ For those stoichiometries that have been considered both in the present work and in ref. 14, *the same structures* were found by both the conventional approach and by the GAs. The GAs offer a higher predictive power and flexibility to identify structures in the regime of large size-disparity and high C -values, where the unit cells become increasingly complex and conventional methods reach their limitations.^{14,15}

If the interaction potentials of eqn (1) were pure power-laws, as those employed in ref. 14, the overall density ηd_A^2 would be an irrelevant parameter, in view of the absence of any length scale in the interactions. Since the logarithmic dependence, as well as the hard cores of the present interactions, eqn (1), set in at very small separations [*cf.* Fig. 2(b)], we expect that the structures reported in Fig. 3 and 4 will be stable for a broad range of small to intermediate densities. To check this assumption, we have investigated the ordered equilibrium configurations of our system varying the density ηd_A^2 from 0.2 to 0.8. We report selected results in Fig. 5. For concentration $C = 1/3$, upper row, the lane-like structure remains unchanged up to a density at least as high as $\eta d_A^2 = 0.6$, only the distances are scaled as η increases. As the density is further increased to $\eta d_A^2 = 0.8$, the following structural transition takes place: every second B-lane is dissolved by merging one of the neighboring ones; consequently, the inter-lane distance and the density in each of these lanes is increased by a factor of two. For $C = 5/6$, a structural change induced by density sets in earlier, namely between $\eta d_A^2 = 0.4$ and $\eta d_A^2 = 0.6$. Here, the original pattern shows rings of B-particles while, again, at high densities lane formation is observed. Moreover,

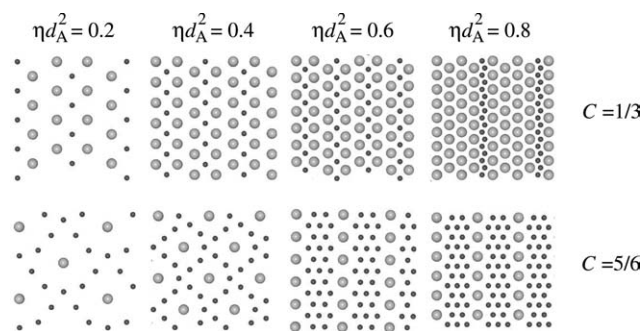


Fig. 5 Two sequences of MECs for $z = 0.5$ and two different concentrations C . Structural change is observed in both sequences, once between $\eta d_A^2 = 0.6$ and $\eta d_A^2 = 0.8$ (top) and once between $\eta d_A^2 = 0.4$ and $\eta d_A^2 = 0.6$ (bottom).

all structures shown here have the lowest energy values found by the GA but, at the same time, other ones with very small energy differences have been discovered in some GA runs. Both the effects of the density and the discussion of 'quasi-degenerate' ground states will be the subject of a future publication.

We have applied genetic algorithms to examine ordered equilibrium configurations for binary, two-dimensional dipolar mixtures. Despite the simplicity of the interactions involved, the system shows a tremendous variety and complexity of the resulting structures. This convincingly demonstrates the power of this novel optimization technique to deal with the problem of finding the global minimum of a rugged potential energy surface, which becomes increasingly involved as the number of components of the mixture increases. We have demonstrated that GAs are an effective and reliable new tool which merits a more widespread appreciation in the soft matter community, on equal footing with complementary tools, such as Monte Carlo simulated annealing and molecular dynamics simulations. The variety of the encountered structures can easily be verified experimentally considering either a binary mixture of two-dimensional superparamagnetic colloidal particles^{9,10} or a binary mixture of polystyrene spheres floating on an oil-water interface.²

Acknowledgements

The authors thank Dieter Gottwald for helpful discussions. This work has been supported by the Austrian Research Foundation (FWF), project numbers P17823-N08 and P19890-N16, and the European Science Foundation short-visit-grant "SimBioMa 1730" (J.F.), by the Marie Curie program of the European Union, contract number MRTN-CT2003-504712 and the Foundation Blanceflor Boncompagni-Ludovisi, née Bildt (F.L.V.), as well as by the DFG within the SFB-TR6, Project Section C3. C.N.L. wishes to thank the Erwin Schrödinger Institute (Vienna), where parts of this work have been carried out, for a Senior Research Fellowship and for its hospitality.

Notes and references

- 1 F. Bresme and M. Oettel, *J. Phys.: Condens. Matter*, 2007, **19**, 413101.
- 2 R. Aveyard, J. Clint, D. Nees and V. Paunov, *Langmuir*, 2000, **16**, 1969.

- 3 R. Aveyard, J. Clint, D. Nees and N. Quirke, *Langmuir*, 2000, **16**, 8820.
- 4 T. Stirner and J. Sun, *Langmuir*, 2005, **21**, 6636.
- 5 K. Zahn, J. M. Méndez-Alcaraz and G. Maret, *Phys. Rev. Lett.*, 1997, **79**, 175.
- 6 K. Zahn, R. Lenke and G. Maret, *Phys. Rev. Lett.*, 1999, **82**, 2721.
- 7 K. Zahn and G. Maret, *Phys. Rev. Lett.*, 2000, **85**, 3656.
- 8 K. Zahn, A. Wille, G. Maret, S. Sengupta and P. Nielaba, *Phys. Rev. Lett.*, 2003, **90**, 155506.
- 9 N. Hoffmann, F. Ebert, C. N. Likos, H. Löwen and G. Maret, *Phys. Rev. Lett.*, 2006, **97**, 078301.
- 10 N. Hoffmann, C. N. Likos and H. Löwen, *J. Phys.: Condens. Matter*, 2006, **18**, 10193.
- 11 J. Sun and T. Stirner, *Langmuir*, 2001, **17**, 3103.
- 12 Another choice is to assume that the dipolar moment scales with the surface area of the spheres, $P_i = \alpha R_i^2$, but we focus on $P_i = \alpha R_i^3$ in this work.
- 13 B. Groh and S. Dietrich, *Phys. Rev. Lett.*, 1997, **79**, 749; B. Groh and S. Dietrich, *Phys. Rev. E*, 1997, **55**, 2892; B. Groh and S. Dietrich, *Phys. Rev. E*, 1998, **57**, 4535; I. Szalai and S. Dietrich, *Mol. Phys.*, 2005, **103**, 2873.
- 14 L. Assoud, R. Messina and H. Löwen, *Europhys. Lett.*, 2007, **80**, 48001.
- 15 C. N. Likos and C. L. Henley, *Philos. Mag. B*, 1993, **68**, 85.
- 16 S. Forrest, *Science*, 1993, **261**, 872.
- 17 J. Holland, *Adaption in Natural and Artificial Systems*, The University of Michigan Press, Ann Arbor, 1975.
- 18 D. M. Deaven and K. M. Ho, *Phys. Rev. Lett.*, 1995, **75**, 288.
- 19 K. M. Ho, A. A. Shvartsburg, B. Pan, Z.-Y. Lu, C.-Z. Wang, J. B. Wacker, J. L. Fye and M. F. Jarrold, *Nature*, 1998, **392**, 582.
- 20 S. M. Woodley, P. D. Battle, J. D. Gale and C. R. A. Catlow, *Phys. Chem. Chem. Phys.*, 1999, **1**, 2535.
- 21 A. Oganov and C. Glass, *J. Chem. Phys.*, 2006, **124**, 244704.
- 22 P. Siepmann, C. Martin, I. Vancea, P. Moriarty and N. Krasnogor, *Nano Lett.*, 2007, **7**, 1985.
- 23 J. Fornleitner and G. Kahl, *Europhys. Lett.*, 2007, submitted; arXiv: 0709.0201.
- 24 D. Gottwald, C. N. Likos, G. Kahl and H. Löwen, *Phys. Rev. Lett.*, 2004, **92**, 068301.
- 25 D. Gottwald, C. N. Likos, G. Kahl and H. Löwen, *J. Chem. Phys.*, 2005, **122**, 074903.
- 26 B. M. Mladek, D. Gottwald, G. Kahl, M. Neumann and C. N. Likos, *Phys. Rev. Lett.*, 2006, **96**, 045701; B. M. Mladek, D. Gottwald, G. Kahl, M. Neumann and C. N. Likos, *Phys. Rev. Lett.*, 2006, **97**, 019901.
- 27 D. Gottwald, G. Kahl and C. N. Likos, *J. Chem. Phys.*, 2005, **122**, 204503.